Organic-Exchanged Silicotungstic Acid Compounds as Efficient and Environmental-Friendly Catalysts for Synthesis of Glycerol Monolaurate

[1]Li Ran, [1]Deng Yunli, [1]Wu Siliang, [1]Liao Jiayi, [2]Tang Xiujuan, [1]Han Xiaoxiang*

[1]Department of Applied Chemistry, Zhejiang Gongshang University, Hangzhou 310035, China.

[2]College of Environmental Science and Engineering, Zhejiang Gongshang University, Hangzhou, 310018, China.

hxx74@126.com*

(Received on 2nd February 2022, accepted in revised form 1st September 2022)

Summary: A series of organic-exchanged silicotungstic acid catalysts were synthesized by changing the variety and amount of organic compounds. The structure, thermal stability and acidic properties of the catalysts were characterized by FT-IR, XRD, TGA and ^{31}P-MAS NMR. The catalytic performances of the catalysts were investigated on the selective esterification of lauric acid with glycerol to glycerol monolaurate. Among the various catalysts, $[QuH]_1H_3SiW_{12}O_{40}$ with molar ratio of quinoline to silicotungstic acid of 1:1 showed excellent activity and reusability due to strong Brønsted acidity and "pseudo-liquid" catalytic modes. The optimal conditions optimized by response surface methodology were as follows: the molar ratio of glycerol to lauric acid was 5.3:1, the amount of catalyst was 4.8 wt%, the reaction temperature was 424 K, and the reaction time was 1.5 h. Under these conditions, the average yield of glycerol monolaurate was 79.7%, which was basically consistent with the values predicted by the mathematical model. Moreover, the kinetic data of this reaction were fitted to a second-order kinetic model and the apparent activation energy E_a was 52.35 kJ / mol.

Keywords: Glycerol monolaurate; Organic exchanged; Esterification; Silicotungstic acid; Kinetic model.

Introduction

Fatty acid monoglycerides with two configurations (α and β) have been considered as an excellent surfactant or emulsifier due to its lipophilicity and hydrophilicity, which is widely used in food, medicine, cosmetics, plastics and other fields [1-3]. As a fatty acid monoglyceride, glycerol monolaurate (GML) is one of the most common surfactants. However, when the content of GML reaches above 90%, it shows not only emulsifying property, but also excellent antibacterial activity which is not easily affected by pH. In 2008, GML was approved as a food additive by the Ministry of Health of the People's Republic of China [5-7]. In addition to antibacterial properties [8, 9], GML also has a certain effect on regulating immune function [10, 11].

The industrial methods of producing fatty acid monoglycerides mainly include direct esterification method, transesterification method, glycidyl method and group protection method [12]. Among them, direct esterification method has attracted much attention due to its simple operational process. In addition, the commonly used catalysts for this method are strong protonic acid, zeolite molecular sieve [13, 14], ion exchange resin [15], ionic liquid [16], metal oxide [17], heteropoly acid [18, 19] and enzyme [20, 21]. Although the above catalysts play a great catalytic role in the preparation of fatty acid monoglycerides, they are still facing some challenges, such as strong corrosion, high cost, serious environmental pollution, difficulty in separation of catalyst and high energy consumption. Therefore, it is of great theoretical and practical significance to develop simple, environmental-friendly and highly effective catalysts for the preparation of fatty acid monoglycerides.

Heteropoly acid is a solid acid with characteristics of strong acidity, easy oxidation and environmental-friendly performance. The adjustable catalytic properties and the "pseudo-liquid" catalytic modes make heteropoly acid a good catalytic candidate for esterification, oxidation and acetalization, etc [22]. However, the practical application of heteropoly acids is limited due to its small specific surface area and solubility during reaction in polar solvents process, which makes the further separation more difficult. To resolve these drawbacks, heteropoly acids have been modified by

*To whom all correspondence should be addressed.

organic compounds to form inorganic-organic hybrid materials, by exchange of metal ion to form insoluble salts, or by dispersing on porous solid supports [21-24]. The prepared inorganic-organic hybrid materials not only have strong acidity, but also have the "self-separation" characteristic that makes the separation process simpler. These novel catalysts offer an environmentally benign process without the drawbacks of equipment corrosion, waste production, and high cost. Therefore, these inorganic-organic hybrid materials have been used widely as catalysts in esterification and acetalization reaction [23-26].

In this paper, the inorganic-organic hybrid materials were synthesized by a series of nitrogen-containing organic compounds and silicotungstic acid (STA), and their structures were characterized by FT-IR, XRD, TGA and ^{31}P solid-state nuclear magnetic resonance. The catalytic performance of the inorganic-organic hybrid materials in the selective esterification of lauric acid (LA) and glycerol (GL) was investigated. On the basis of single factor experiments, response surface methodology (RSM) was used to optimize the synthesis process of GML and the kinetic model under the optimal reaction conditions was established, which provided theoretical base for the large-scale production of GML.

Experimental

Catalyst preparation

All the chemicals were used directly without further purification. A series of organic-exchanged STA catalysts have been prepared, and the preparation process of quinoline-exchanged STA acid was taken as an example. The specific detail of the preparation is as follows: 2.88 g (1 mmol) of calcined STA and 30 mL of deionized water with appropriate amount of quinoline (Qu) were mixed into a 100 mL three-necked flask and stirred overnight at 363 K. After the reaction, the water was evaporated and the solid compounds were washed with ether for 3 times. Then the samples were dried in vacuum at 348 K for 8 h to obtain a series of Qu-exchanged STA catalysts, which were recorded as $[QuH]_xH_{4-x}SiW_{12}O_{40}$, where *x* represented the ratio of Qu to STA (x=1, 2, 3 and 4). The reaction equation (1) of catalyst preparation is as follows:

$$x\mathrm{Qu} + H_4SiW_{12}O_{40} \rightarrow [QuH]_xH_{4-x}SiW_{12}O_{40} \ (x = 1\sim4) \quad (1)$$

Catalyst characterization

Fourier-transform infrared spectra (FT-IR) was detected by the model of Bruker Vertex 70 spectrometer using KBr pellet method. The structural properties of various catalysts were analyzed by recording the wavenumber in the range of 4000-400 cm^{-1}. X-ray diffraction (XRD) profiles were obtained by the model of Rigaku Ultimate IV X-ray diffractometer with Cu K_α radiation at 40 kV and 10 mA. The XRD patterns were acquired in the 2θ range of 5-80° at an interval of 0.04 °/min. The thermal stabilities of these catalysts were characterized by the model of TGA/DSC-1（METTLER）thermal analyzer. The samples were heated under N_2 atmosphere from room temperature to 873 K at heating rates of 20 K/min.

Acidic property is one of the important indexes of catalyst. In this study, solid-state ^{31}P TMPO nuclear magnetic resonance (^{31}P-TMPO MAS-NMR）was used to characterize the detailed acid properties by the model of Bruker Avance III 500 spectrometer. Trimethylphosphine oxide (TMPO) was used as a basic probe molecule to determine the type of acid (Brønsted acid and Lewis acid), distribution, number and strength of acid sites on solid catalyst by detecting the change of ^{31}P chemical shift.

Esterification reaction

LA (0.05 mol), GL (0.25 mol) and 0.5 g catalyst were added into a 100 mL three-necked flask equipped with a condensation reflux device and a mechanical stirring device. The reaction mixture was heated for a period of time in an oil bath. Then the reaction products were analyzed by the model of Agilent GC 7890B gas chromatography using a flame ionization detector (FID) and a HP-5 capillary column. The column temperature was ramped from 373 K to 573 K at a rate of 25 K/min and maintained for 10 min with methyl laurate as the internal standard. The GML yield was determined by the equation (2):

$$\text{GML yield (\%)} = \text{LA conversion (\%)} \times \text{GML selectivity (\%)} \quad (2)$$

Experimental design and mathematical model

On the basis of Box-Behnken design (BBD), response surface methodology (RSM) was used to

optimize the reaction process in order to get higher GML yield in the selective esterification reaction. Three independent variables were selected, namely, the molar ratio of GL/LA (x_1), the amount of catalyst (x_2), and reaction temperature (x_3), at three coded levels -1 (low value), 0 (central value) and +1 (high value), as shown in Table 1. In this paper, 17 experimental sets were carried out (including 12 factorial points and 5 central tests) with 3^3 full-factorial central composite design, as shown in Table 2. The coded values of these factors were obtained by the equation (3):

$$x_i = \frac{X_i - X_0}{\Delta X_i} \quad (3)$$

where x_i, X_i and X_0 (i = 1-3) represented the coded, real and central value of the independent variables respectively, and ΔX_i indicated the step-change value of the associated variable. In order to get the optimized reaction process and predict the yield of GML, a second-order RSM mathematic model was used to indicate the interactive effects between different process variables and the quadratic equation (4) may be expressed as follows:

$$Y = \beta_0 + \sum_{i=1}^{3} \beta_i x_i + \sum_{i=1}^{3} \beta_{ii} x_i^2 + \sum_{i<j}^{3} \beta_{ij} x_i x_j \quad (4)$$

where Y represented the predicted response, x_i and x_j (i and j = 1-3) indicated the uncoded independent variables, while β_0, β_i, β_{ii}, and β_{ij} denoted the regression coefficients of the offset, linear, quadratic and interactive term for the corresponding variables respectively.

Kinetic studies

Under the conditions of this study, the main target product was GML, while a small amount of glycerol dilaurate (GDL) was obtained, and glyceryl laurate was not detected. Therefore, the chemical reaction process of selective preparation of GML by esterification of LA with GL can be simplified as follows:

$$LA + GL \leftrightarrow GML + H_2O$$

Table-1: Experimental factor and range levels for esterification process.

Factors (unit)	Symbol	Range and levels		
		-1	0	1
GL/LA molar ratio (moL/moL)	x_1	4.5	5.0	5.5
Catalyst amount (wt%)	x_2	4.0	5.0	6.0
Reaction temperature (K)	x_3	413	423	433

Table-2: The design scheme and results of response surface methodology.

Run	Variable and value			GML yield (%)	
	x_1	x_2	x_3	Experimental	Predicted
1	4.50	4.00	423.00	74.95	75.09
2	5.50	4.00	423.00	77.98	78.55
3	4.50	6.00	423.00	75.09	74.52
4	5.50	6.00	423.00	76.48	76.34
5	4.50	5.00	413.00	68.53	68.73
6	5.50	5.00	413.00	75.42	75.19
7	4.50	5.00	433.00	77.06	77.29
8	5.50	5.00	433.00	76.31	76.11
9	5.00	4.00	413.00	74.31	73.97
10	5.00	6.00	413.00	68.82	69.19
11	5.00	4.00	433.00	75.69	75.32
12	5.00	6.00	433.00	76.98	77.32
13	5.00	6.00	423.00	78.94	78.60
14	5.00	5.00	423.00	79.14	78.60
15	5.00	5.00	423.00	78.56	78.60
16	5.00	5.00	423.00	78.29	78.60
17	5.00	5.00	423.00	78.07	78.60

The rate equation during the esterification of GL with LA might be defined as:

$$r = -\frac{dc_A}{dt} = k_+ c_A^{\alpha} c_B^{\beta} - k_- c_C^{\gamma} c_D^{\eta} \quad (5)$$

where C_A, C_B, C_C, and C_D represented the concentration of LA, GL, GML, and H_2O respectively; k_+ and k_- denoted the forward and reverse rate constants respectively; α, β, γ, and η were the reaction order of LA, GL, GML, and H_2O respectively. Because GL and LA were equimolar reactions, and the amount of GL used in the reaction was far greater than that of LA, it could effectively promote the reaction equilibrium to move into the positive direction and inhibit the reverse reaction. Therefore, the reaction was supposed to be regarded as an irreversible reaction. The rate equation (5) could be simplified as:

$$r = -\frac{dc_A}{dt} = kc_A^{\alpha} c_B^{\beta} \quad (6)$$

Owing to the "pseudo-liquid" catalytic modes of Qu-exchanged STA catalyst, the esterification reaction could be described by a pseudo homogeneous second-order kinetic model [27]. Supposed $\alpha = \beta = 1$, $Q = C_{B0} - C_{A0}$, where C_{A0} and C_{B0} represented the initial concentration of LA and GL respectively, then $C_B = C_A + Q$, and the formula (6) could be rewritten as:

$$r = -\frac{dc_A}{dt} = kc_A(c_A + Q) \quad (7)$$

Integrated the two sides of the formula and got the new formula (8) as:

$$\ln\frac{c_A}{c_B} = (c_{A0} - c_{B0})kt + C \quad (8)$$

The relationship between ln (C_A/C_B) and time could be fitted by the formula (8), and then the modified reaction rate k at different temperatures could be obtained. Then, the pre-exponential factor k_0 and activation energy E_a of the esterification reaction might be calculated.

$$\ln k = \ln k_0 - \frac{E_a}{R}\frac{1}{T} \quad (9)$$

Results and Discussion

Characterization of catalysts

FI-IR spectra of $H_4SiW_{12}O_{40}$, Qu and Qu-exchanged STA were depicted in Fig. 1. In accordance with the previous studies, five apparent characteristic bands of pristine STA (Fig. 1a) could be obtained at about 3437, 979, 925, 879 and 791 cm^{-1}, which could be assigned to the vibrational modes of O-H, W-O_a (terminal), Si−O_b, W−O_c−W (corner sharing) and W−O_d−W (edge sharing) [28] respectively, and the last four were the characteristic bands of Keggin anions. Fig. 1 (c-f) showed the FT-IR spectra of STA modified by Qu with different ratios. Similar absorption bands were observed for the Qu-exchanged STA composites despite marginal variations in peak indicating that the incorporation of Qu didn't change the basic framework structure of $H_4SiW_{12}O_{40}$.

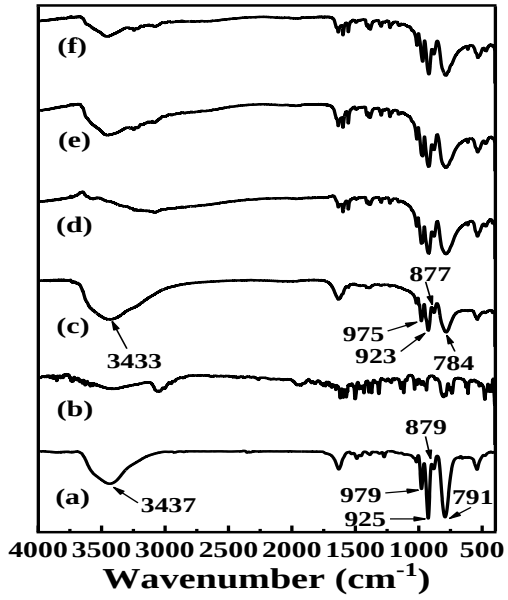

Fig.1: FT-IR spectra of (a) $H_4SiW_{12}O_{40}$, (b) Quinoline, (c) $[QuH]_1H_3SiW_{12}O_{40}$, (d) $[QuH]_2H_2SiW_{12}O_{40}$, (e) $[QuH]_3H_1SiW_{12}O_{40}$, (f) $[QuH]_4SiW_{12}O_{40}$.

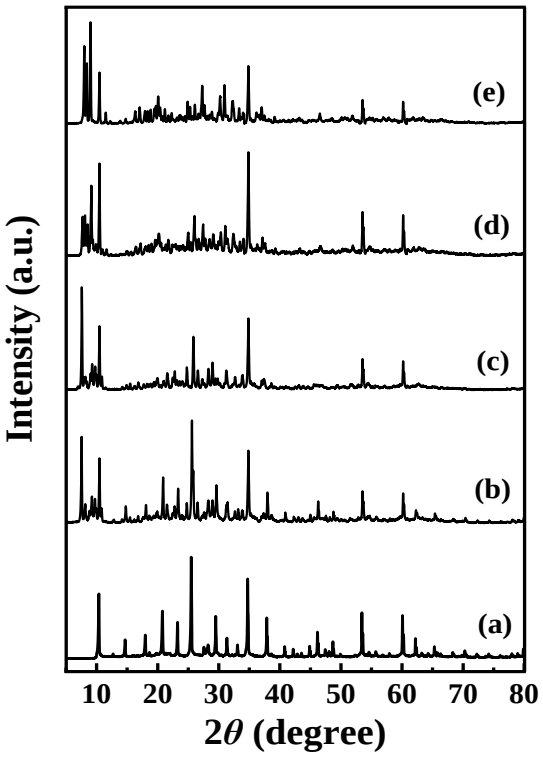

Fig. 2: XRD patterns of (a) $H_4SiW_{12}O_{40}$, (b) $[QuH]_1H_3SiW_{12}O_{40}$, (c) $[QuH]_2H_2SiW_{12}O_{40}$, (d) $[QuH]_3H_1SiW_{12}O_{40}$, (e) $[QuH]_4SiW_{12}O_{40}$.

Fig. 2 displayed the XRD patterns of the pristine STA and various Qu-exchanged STA catalysts. The pristine STA had three apparent diffraction peaks at 10.3º, 25.3º and 34.6º which were similar to previous reports [29]. As shown in Fig. 2(b-e), with the adding of Qu, similar diffraction peaks could be obtained despite a little variation in peak and change in intensity, indicating that the addition of Qu didn't change the Keggin structure of STA. The results were consistent with the FI-IR analysis. Moreover, a series of new diffraction peaks appeared at 2θ of 5-10º (Fig. 2(b-e)) which might partly due to the internal chemical bond of Qu group, and partly because of the interaction between Qu and STA forming a new chemical bond.

The thermal stability of catalyst is an important index to measure the excellent performance of catalyst and TGA-DTG can be used to analyze the thermal stability of catalyst intuitively. Since the preparation method of various organic-exchanged STA was the same, their TGA-DTG patterns were also similar. Therefore, only TGA-DTG diagrams of STA, Qu and $[QuH]_1H_3SiW_{12}O_{40}$ were illustrated and discussed here. As shown in Fig. 3a, the pristine STA showed three apparent weight loss peaks at 321, 459, and 670-825 K, which might be assigned to desorption of physically adsorbed water, loss of crystal water and collapse of Keggin structure respectively. The weight loss peak at 558 K corresponded to the decomposition of Qu. As shown in Fig. 3c, during the heating process of $[QuH]_1H_3SiW_{12}O_{40}$, there were four obvious weight loss peaks at 324, 376, 560 and 765-819 K, which might be ascribed to the separation of adsorbed water on the catalyst surface, the loss of crystal water, the decomposition of organic components and the collapse of Keggin structure of $[QuH]_1H_3SiW_{12}O_{40}$. Consequently, the $[QuH]_1H_3SiW_{12}O_{40}$ catalyst had a relatively stable structure and could maintain good thermal stability in the reaction system for the preparation of GML.

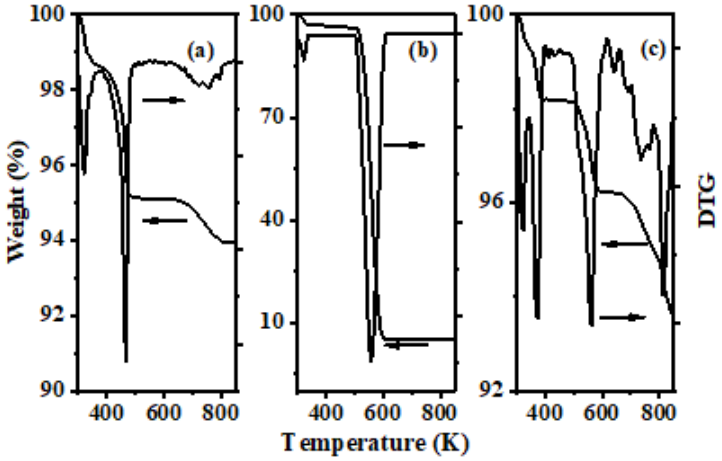

Fig. 3: TGA-DTG profiles of (a) $H_4SiW_{12}O_{40}$, (b) Quinoline, and (c) $[QuH]_1H_3SiW_{12}O_{40}$.

Compared with traditional acid determination methods, ^{31}P-TMPO MAS-NMR can provide important acidic characteristics for various catalysts. For all kinds of solid and liquid acid catalysts, detailed acid properties can be obtained at the same time, such as the acid type, concentration, distribution and strength of acid sites [30, 31]. Therefore, ^{31}P-TMPO MAS-NMR can be used as an effective tool to study the acidity of solid catalysts. As an important basic probe molecule, TMPO was used to characterize the acidity of solid catalysts. It mainly formed $(TMPO)_nH^+$ complex by adsorbing acidic protons on the catalyst and the $(TMPO)_nH^+$ complexes formed by different acidic catalysts and probe molecules were different, and thus showed different ^{31}P chemical shifts, namely acid types and strength. Fig. 4 displayed the ^{31}P MAS NMR spectrum of pristine STA and various Qu-exchanged STA catalysts. The pristine STA (Fig.4a) exhibited overlapping resonance peaks at 88 ppm and 90 ppm which corresponded to the solid superacid of $H_4SiW_{12}O_{40}$ [32]. As shown in Fig. 4 (b-e), the results of various Qu-exchanged STA catalysts showed that there were obvious resonance peaks in the range of 80-95 ppm indicating that the Qu-exchanged STA catalysts still retained the original strong acid sites of $H_4SiW_{12}O_{40}$. With the increasing of Qu content in the catalyst, the resonance peak intensity corresponding to strong acid gradually decreased, demonstrating that the acidity of the catalysts decreased gradually. In addition, a new broad peak appeared in the region of 40-60 ppm for $[QuH]_3H_1SiW_{12}O_{40}$ and $[QuH]_4SiW_{12}O_{40}$ catalysts. The main reason for this phenomenon was that Qu could stretch the lattice of $H_4SiW_{12}O_{40}$, which made ^{31}P-TMPO easy to transfer and disperse in the STA lattice [26].

Esterification reaction

Table 3 showed the catalytic performances of various organic-exchanged STA catalysts for selective esterification of GL with LA to produce GML. In the absence of catalyst, the conversion of LA was 51.5%, which indicated that the reaction was autocatalytic and LA played an acid catalytic role in the reaction process, but the overall catalytic activity was low. Apparently the pristine $H_4SiW_{12}O_{40}$ had higher LA conversion and GML yield than pristine $H_3PW_{12}O_{40}$. Therefore, $H_4SiW_{12}O_{40}$ was used as the main structural unit and exchanged by various organics to study the catalytic activity. Among various catalysts, $[QuH]_1H_3SiW_{12}O_{40}$ catalyst exhibited good catalytic activity and the highest GML yield (78.9%) while LA conversion was 90.7%. The catalytic performance of Qu-exchanged STA catalysts in selective esterification was further investigated and the results showed that the catalytic activity of these catalysts decreased with the increase of Qu content. The reason was that the steric hindrance inside the crystal structure of catalyst would increase due to the high content of Qu, which hindered the movement of reactant molecules. In other words, the effective collision between molecules was reduced leading to the decrease of GML yield. The pristine $H_4SiW_{12}O_{40}$ had the strongest Brønsted acidity, and the corresponding Brønsted acidity of the catalyst decreased with the increasing of Qu content, which indicated that stronger acidity didn't mean the higher yields in the selective esterification reaction. Too high Brønsted acidity would aggravate the occurrence of side reactions such as further esterification and ester hydrolysis. During the esterification reaction catalyzed by inorganic-organic hybrid materials, the catalyst was a solid in the initial reaction. Since the catalyst was completely dissolved in glycerol and water, the reaction system was strictly uniform. With the progress of the reaction, the reaction mixture gradually became turbid milky. After the reaction was completed, the high yield of the ester led to the spontaneous self-separation between the product and catalyst. The "pseudo-liquid" and "self-separation" characteristics of the Keggin structure were of great benefit to the activity of this kind of catalysts.

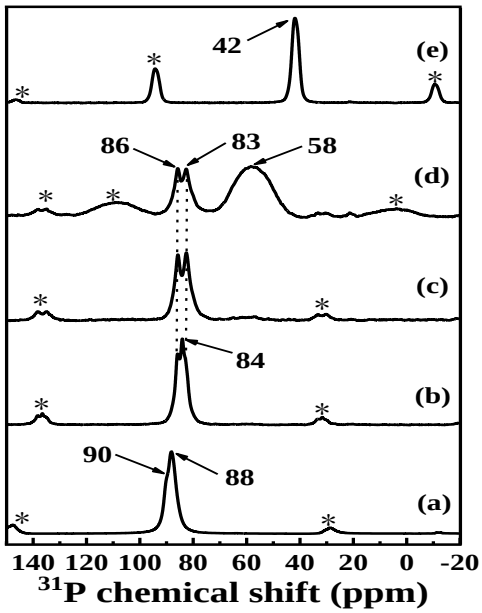

Fig. 4: ^{31}P NMR spectra for (a) $H_4SiW_{12}O_{40}$, (b) $[QuH]_1H_3SiW_{12}O_{40}$, (c) $[QuH]_2H_2SiW_{12}O_{40}$, (d) $[QuH]_3H_1SiW_{12}O_{40}$, (e) $[QuH]_4SiW_{12}O_{40}$.

Table-: The catalytic activity of different solid acid catalysts in the preparation of GML [a]

Entry	Calalyst	Selectivity (%)			LA conversion (%)	GML yield (%)
		GML	GDL	GTL		
1	Blank	70.0±1.2	30.0±1.2	nil	50.4±1.1	35.3±0.6
2	Quinoline	76.6±0.8	23.4±0.8	nil	71.0±0.9	54.4±0.6
3	$H_4SiW_{12}O_{40}$	80.5±0.7	19.5±0.7	nil	89.8±1.0	72.3±0.6
4	$H_3PW_{12}O_{40}$	78.1±1.0	21.9±1.0	nil	87.8±1.2	68.6±0.9
5	$[QuH]_1H_3SiW_{12}O_{40}$	87.0±0.8	13.0±0.8	nil	90.7±1.1	78.9±0.7
6	$[QuH]_2H_2SiW_{12}O_{40}$	85.8±0.7	14.2±0.7	nil	85.9±0.9	73.7±0.6
7	$[QuH]_3H_1SiW_{12}O_{40}$	84.8±1.1	15.2±1.1	nil	80.7±0.7	68.4±0.9
8	$[QuH]_4SiW_{12}O_{40}$	78.8±0.9	21.2±0.9	nil	67.4±1.1	53.1±0.6
9	$[DMAH]_1H_3SiW_{12}O_{40}$	85.7±0.6	14.3±0.6	nil	90.3±0.6	77.4±0.9
10	$[DMBH]_1H_3SiW_{12}O_{40}$	83.3±1.2	12.6±1.2	nil	87.5±0.8	72.9±1.0
11	$[TEAH]_1H_3SiW_{12}O_{40}$	86.6±1.1	13.4±1.1	nil	89.0±0.9	77.1±1.0
12	$[TBAH]_1H_3SiW_{12}O_{40}$	80.8±0.9	14.3±0.9	nil	95.6±0.5	77.2±0.9
13	$[PyH]_1H_3SiW_{12}O_{40}$	87.0±1.3	13.0±1.3	nil	79.9±1.2	69.5±1.1
14	$[DMPyH]_1H_3SiW_{12}O_{40}$	86.3±0.7	13.7±0.7	nil	85.3±1.1	73.6±0.6
15	$[EMPyH]_1H_3SiW_{12}O_{40}$	85.2±1.1	14.8±1.1	nil	86.0±0.9	73.3±0.9
16	$[PiH]_1H_3SiW_{12}O_{40}$	83.2±0.8	16.8±0.8	nil	93.4±1.3	77.7±0.8
17	$[CDIH_2]_{1/2}H_3SiW_{12}O_{40}$	87.2±0.7	12.8±0.7	nil	87.2±1.1	76.0±0.6

[a]Reaction conditions: GL/LA molar ratio = 5 (moL/moL); catalyst amount (relative to LA) = 4 wt%; reaction time = 1.5 h; reaction temperature = 423 K.

Effects of reaction parameters on the catalyst performance

Using $[QuH]_1H_3SiW_{12}O_{40}$ as the catalyst, the effects of the molar ratios of GL/LA, the amount of the catalyst, reaction temperature and reaction time on the synthesis of GML were investigated, as shown in Fig. 5.

The selective esterification of LA and GL is a continuous and reversible reaction. Increasing the amount of GL can promote the reaction toward the positive direction, so as to improve the conversion of LA and the yield of GML. Under the conditions of catalyst amount = 4 wt%, reaction temperature = 423 K and reaction time = 1.5 h, the effect of the molar ratio of GL/LA was investigated. As shown in Fig. 5a, with the increasing of GL/LA molar ratio, namely increasing the amount of GL, the conversion of LA increased to the maximum value (91.7%) and then decreased slowly. When the molar ratio of GL/LA was 5:1, GML yield reached the maximum value of 77.1%. Further increasing the molar ratio of GL/LA would dilute the relative concentration of the catalyst and affect the forward reaction, leading to the conversion of LA and yield of GML decreasing. Therefore, the optimum of GL / LA molar ratio is 5:1.

Esterification is a typical acid catalyzed reaction. If the amount of catalyst was increased, the available active sites and catalytic activity were supposed to increase [33]. As shown in Fig. 5b, under the conditions of the molar ratio of GL/LA = 5:1, reaction temperature = 423 K and reaction time = 1.5 h, the effect of the amount of catalyst was investigated. With the amount of catalyst varying from 2 to 6 wt%, the conversion of LA continued to increase, while the yield of GML increased first and then decreased. When the amount of catalyst was 5 wt%, the maximum GML yield was 78.6%, suggesting the suitable amount of catalyst would lead to the increase of active sites. However, the excessive catalyst would lead to the occurrence of the side reactions such as further esterification resulting in the decrease of the selectivity and yield of GML. Therefore, the optimum of catalyst amount is 5 wt%.

Generally, with the increase of temperature, the collision frequency between reactants increases, therefore, the reaction rate increases [34]. As shown in Fig. 5c, under the conditions of the molar ratio of GL/LA = 5:1, the amount of catalyst = 5 wt% and reaction time = 1.5 h, the conversion of LA increased continuously from 82.9% to 97.3% during the reaction temperature of 403 ~ 443 K, and the maximum GML yield reached 78.6% at 423 K. As mentioned above, increasing temperature accelerated the reaction process, but too high temperature promoted the occurrence of side reactions, namely the conversion of GML to GDL and the yield of GML reduced. From the perspective of environmental protection and low energy consumption, the reaction temperature was selected as 423 K.

As shown in Fig. 5d, under the conditions of the molar ratio of GL/LA = 5:1, the amount of catalyst = 5 wt% and reaction temperature = 423 K, with the extension of reaction time, the conversion of LA increased gradually and then basically maintained unchanged, while the yield of GML increased first and decreased which reached the maximum of 78.6 % at 1.5 h. When the esterification reached the chemical equilibrium, extending the reaction time would not only lead to the reaction proceed in the reverse direction, but also cause further esterification reaction, resulting in the decrease of GML yield. Therefore, it was appropriate to control the reaction time of 1.5 h.

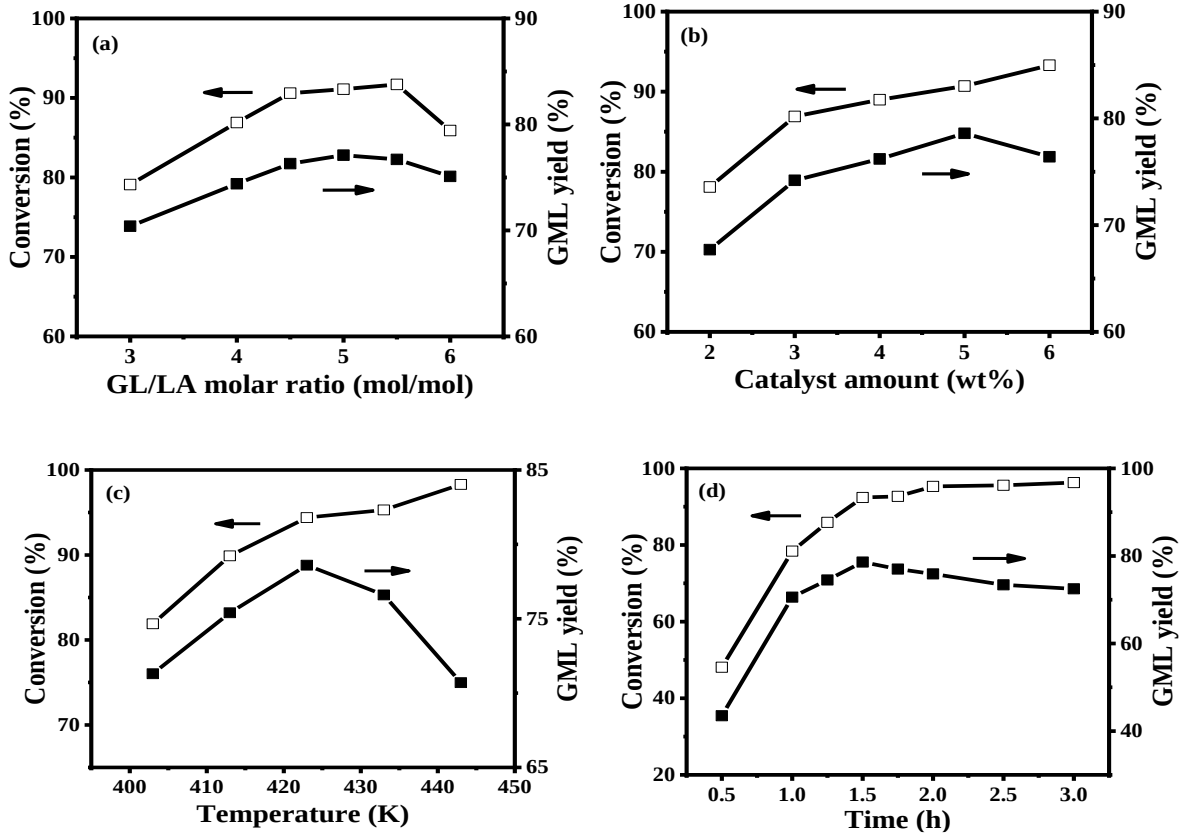

Fig. 5: The influence of different reaction variables on GML's yield over $[QuH]_1H_3SiW_{12}O_{40}$.

Table-4: Analysis of variance table.

Source	Sum of squares	Degree of freedom (DF)	Mean square	*F*-value	*Prob* > *F*	Significance
Model	**151.21**	**9**	**16.80**	**54.31**	**<0.0001**	**
x_1	**13.94**	**1**	**13.94**	**45.06**	**0.0003**	**
x_2	**3.86**	**1**	**3.86**	**12.49**	**0.0095**	**
x_3	**44.94**	**1**	**44.94**	**145.25**	**<0.0001**	**
x_1^2	**4.62**	**1**	**4.62**	**14.93**	**0.0062**	**
x_2^2	**8.58**	**1**	**8.58**	**27.73**	**0.0012**	**
x_3^2	**43.72**	**1**	**43.72**	**141.33**	**<0.0001**	**
x_1x_2	**0.67**	**1**	**0.67**	**2.17**	**0.1839**	
x_1x_3	**14.59**	**1**	**14.59**	**47.17**	**0.0002**	**
x_2x_3	**11.49**	**1**	**11.49**	**37.15**	**0.0005**	**
Residual	**2.17**	**7**	**0.31**			
Lack of Fit	**1.38**	**3**	**0.46**	**2.34**	**0.2146**	**NS**
Pure Error	**0.79**	**4**	**0.20**			
Cor Total	**153.38**	**16**				

RSM experiments and studying

Response surface methodology (RSM), as an effective method, was used to optimize the process variables and predict the response (GML yield), *Y*. The multiple quadratic regression equation (eq10) was established based on the experimental data to show the possible functional relationship between each factor and the response value by an empirical model [35]:

$$Y = + 78.60 + 1.32\ x_1 - 0.70\ x_2 + 2.37\ x_3 - 1.05\ x_1^2 - 1.43\ x_2^2 - 3.22\ x_3^2 - 0.41\ x_1x_2 - 1.91\ x_1x_3 + 1.70\ x_2x_3 \quad (10)$$

where x_i (i = 1-3) were the coded values of the process variables specified in Table 1. In order to verify the model, 12 groups of factorial tests and 5 groups of central tests were carried out and the response value corresponding to each experimental

set was obtained by multiple regression analysis, as depicted in Table-2.

The quality of regression fitting with Equ (10) was evaluated by the analysis of variance (ANOVA) and the results were summarized in Table 4. The *F* value of the model was 54.31, and values of "*Prob* > *F*" less than 0.0001 indicated that model terms were significant. In addition, the mismatch of the quadratic regression model in this experiment was insignificant, namely, the quadratic regression model had high fitting degree and relatively small error. Coefficient of variation (C.V.%) is an absolute value reflecting the degree of data dispersion, and it is also an important parameter to evaluate the rationality of the model. The smaller the value it is, the better result will get. The CV of 0.73% was within the acceptable range, indicating that the experiment had good repeatability. The correlation coefficient square (Pred R^2 = 0.9859; Adj R^2=0.9677) indicated that the model had high reliability. In conclusion, this model could be used to predict the yield of GML.

Fig. 6 contained a three-dimensional surface map and a two-dimensional contour map of the interaction between different factors. The significance of the interaction between different factors could be judged by the shape and density of the contour line. When the contour line was elliptical and dense, the interaction between the two factors was significant; on the contrary, when the contour line was approximately circular and the lines were relatively scattered, it indicated that the interaction between the two factors was not significant.

Figs. 6 (a) and (b) showed the effect of the interaction between the molar ratio of GL/LA and the amount of catalyst on the yield of GML. It could be seen from the figure that the two-dimensional contour line was nearly circular and the distance between lines was large, so the interaction between the molar ratio of GL / LA and the amount of catalyst was insignificant, which was consistent with the results of variance analysis in Table 4. In addition, along the axis direction of x_2 (catalyst amount), when the molar ratio of GL/LA remained at 5.0, the GML yield first increased slowly and then decreased gradually with the increase of catalyst amount. Along the axis direction of x_1 (the molar ratio of GL/LA), the GML yield first increased slowly and then remained unchanged with the increase of the molar ratio of GL/LA when catalyst amount remained at 5 wt%. Relatively speaking, the contour lines in the direction of x_2 axis were denser than those in the direction of x_1 axis, so catalyst amount had a greater effect on the GML yield than the molar ratio of GL/LA.

The effect of the interaction between the molar ratio of GL/LA and reaction temperature on the yield of GML were shown in Figs. 6 (b) and (e). It could be seen from the figure that the contour line was flat ellipse and the contour line along the reaction temperature direction was denser. Therefore, the interaction between the molar ratio of GL/LA and reaction temperature was significant, and the influence of reaction temperature on GML yield was greater.

Figs. 6 (c) and (f) showed the effect of the interaction between catalyst amount and reaction temperature on GML yield. It could be seen from Fig. 6f that the contour lines were elliptical and dense, so the interaction between catalyst amount and reaction temperature was significant, which was consistent with the analysis of variance. In addition, from the three-dimensional curved surface, it could be seen that the surface along the reaction temperature direction was steeper. In another word, the influence of reaction temperature on GML yield was greater than that of catalyst amount.

According to the above RSM analysis, the influence order of the above three factors on GML yield was as follows: reaction temperature > catalyst amount > molar ratio of GL/LA. As a result, the optimum reaction conditions for the selective esterification of LA and GL with $[QuH]_1H_3SiW_{12}O_{40}$ as catalyst were as follows: the molar ratio of GL/LA was 5.27:1, the amount of catalyst was 4.76 wt%, the reaction temperature was 424.44 K, and the reaction time was 1.5 h. Under these conditions, the predicted yield of GML was 79.21%. Considering the convenience of experimental operation, the esterification conditions were modified as follows: the molar ratio of GL/LA was 5.3:1, the amount of catalyst was 4.8 wt%, the reaction temperature was 424 K, and the reaction time was 1.5 h. In order to verify the accuracy of the quadratic regression model, five repeated experiments were carried out under these conditions, and the average yield of GML was 79.7%, which was basically consistent with the theoretical prediction value, indicating that the quadratic regression model can accurately reflect the influence of various factors on the yield of GML.

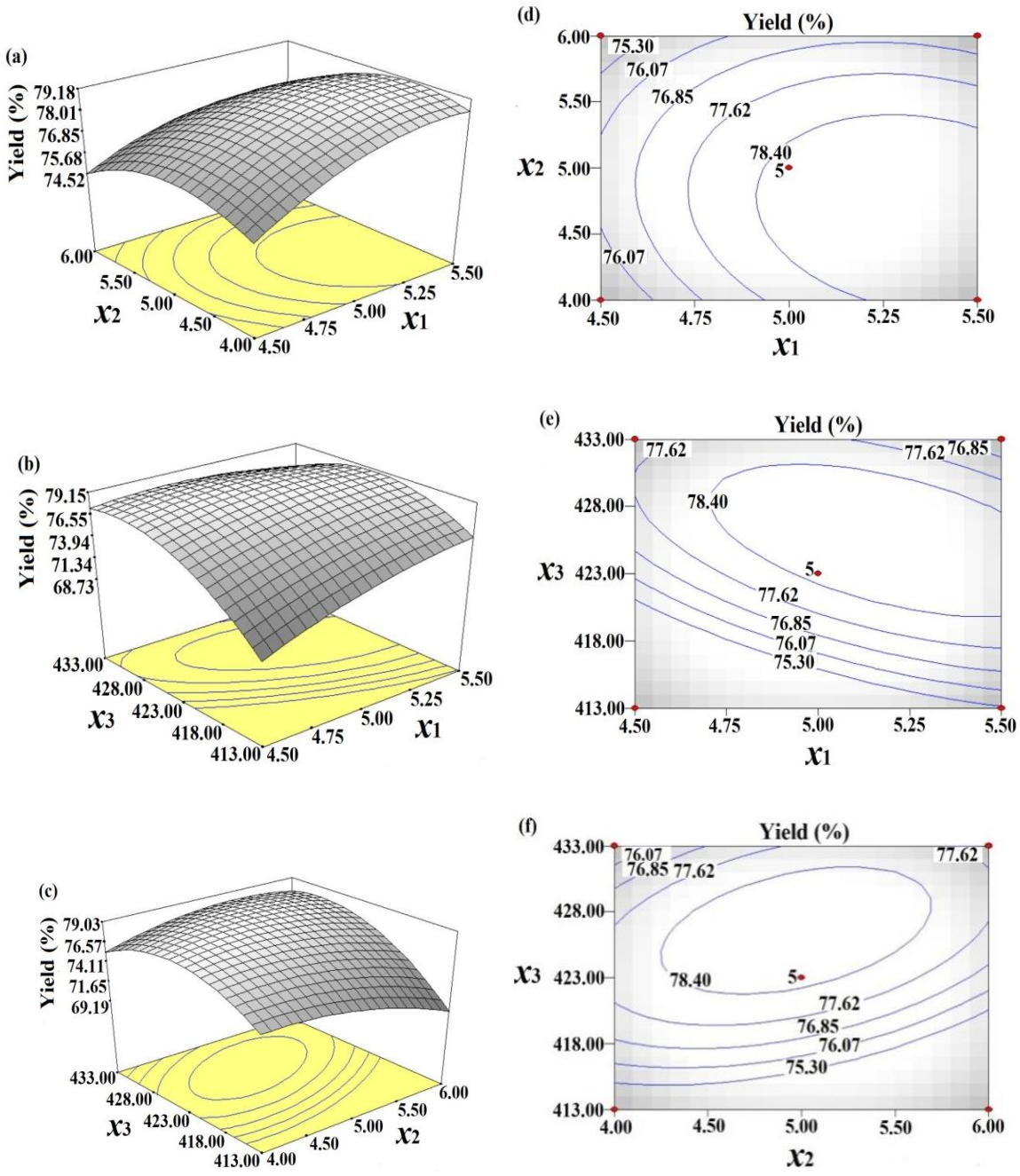

Fig. 6: (a-c) 3D response surface and (d-f) contour plots of the influence of different factors on GML yield.

Recycling of the catalyst

From the perspective of industrial production, the reusability of catalyst is an important index. The reusability of $[QuH]_1H_3SiW_{12}O_{40}$ catalyst was investigated under the above optimal conditions. After the reaction, the reaction system was resting and cooling. The "self-separation" characteristic of $[QuH]_1H_3SiW_{12}O_{40}$ catalyst promoted the catalyst separation from the reaction system, and the catalyst could be easily separated by filtration. Then the catalyst was washed by ether for several times and dried in vacuum at 348 K. The experimental results were shown in Fig. 7. The conversion of LA decreased from 92.7% to 83.2% while the yield of GML decreased from 79.7% to 70.9%. The elemental

analysis of $[QuH]_1H_3SiW_{12}O_{40}$ catalyst reused for six times showed that the mass fraction of Si decreased from 0.93 % (fresh catalyst) to 0.72% (spent catalyst) and the decrease of catalyst activity was related to the loss of active component STA. The results showed that $[QuH]_1H_3SiW_{12}O_{40}$ catalyst had stable structure, good reusability and application value.

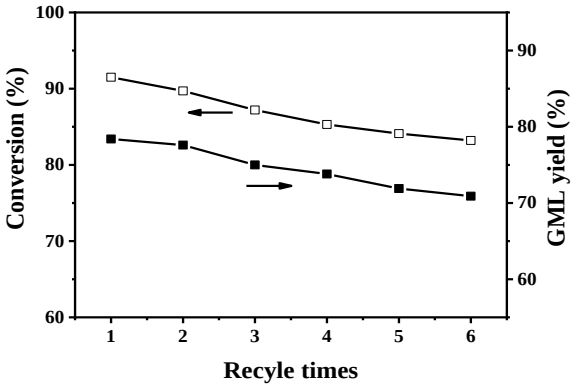

Fig. 7: Catalyst reusability in the esterification of lauric acid with glycerol over $[QuH]_1H_3SiW_{12}O_{40}$ under optimal conditions.

Kinetic model of monoglyceride formation

The kinetics involved in the esterification of GL with LA to GML over the $[QuH]_1H_3SiW_{12}O_{40}$ catalyst was also examined. The experiments were carried out at 413, 418, 423 and 428 K respectively and samples were taken at 30, 45, 60, 75 and 90 min at each temperature. Other reaction conditions were fixed as follows: the molar ratio of GL/LA = 5.3:1, and the amount of catalyst was 4.8 wt%. The relationship between "ln (C_A/C_B)" and "t" at different temperatures was drawn from the data. The results were shown in Fig. 8.

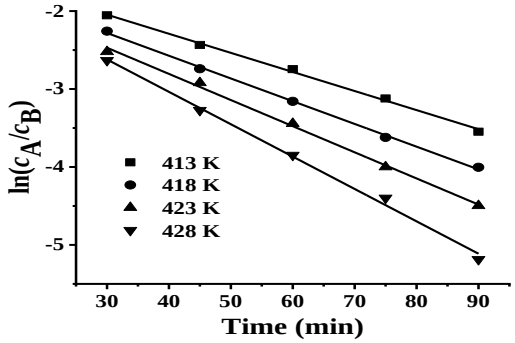

Fig. 8: Plots of ln(c_A/c_B) versus time for the esterification.

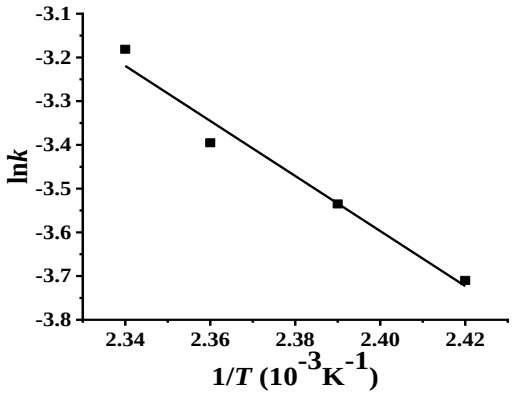

Fig. 9: Arrhenius plots of ln *k* versus 1/*T*.

The reaction rate constant *k* and the correlation coefficients of "ln (C_A/C_B)" with "t" at different temperatures were obtained by linear fitting, with R^2 of 0.9966, 0.9983, 0.9962 and 0.9949 respectively. At the same time, the relationship between ln *k* and 1/T could be obtained by Arrhenius formula (9). The result was shown in Fig. 9 and it was a linear equation with a correlation coefficient of 0.9725, indicating that the esterification reaction was a second-order reaction. According to the intercept and slope, the apparent activation energy E_a = 52.35 kJ/mol and the pre-exponential factor $k_0 = 1.0 \times 10^5$ L/(mol•min). Therefore, under the optimal conditions, the kinetic equation of $[QuH]_1H_3SiW_{12}O_{40}$ catalytic synthesis of GML could be expressed as follows:

$$r = -\frac{dc_A}{dt} = 10^5 exp(-\frac{52.35}{RT})c_A c_B$$

Conclusions

A series of organic-exchanged STA catalysts were successfully synthesized and exploited for production of GML through selective esterification of GL and LA. Among various catalysts, the $[QuH]_1H_3SiW_{12}O_{40}$ catalyst exhibited superior catalytic activity for the high Brønsted acidity and "pseudo-liquid" catalytic modes with a GML yield of 79.7%, which was in close resemblance with the predicted results by the RSM based on the BBD model. The optimized process variables included: the molar ratio of GL/LA = 5.3:1, the amount of catalyst = 4.8 wt%, reaction temperature = 424 K, and reaction time = 1.5 h. In addition, the kinetic studies of synthesizing GML using $[QuH]_1H_3SiW_{12}O_{40}$ as catalyst were carried out and the apparent activation

energy of the reaction was 52.35 kJ / mol. Under the above conditions, the $[QuH]_1H_3SiW_{12}O_{40}$ catalyst could be used for 6 times with the GML yield decreasing from 79.7% to 70.9%, indicating its great stability, recyclability and appliance value for other acid-catalyzed reactions.

References

1. X. X. Han, G. Q. Zhu, Y. X. Ding, *et al*, Selective catalytic synthesis of glycerol monolaurate over silica gel-based sulfonic acid functionalized ionic liquid catalysts, *Chem. Eng. J*., 359, 733 (2019).
2. P. Lozano, C. Gomez, S. Nieto, *et al*, Highly selective biocatalytic synthesis of monoacylglycerides in sponge-like ionic liquids, *Green Chem*., **19**, 390 (2017).
3. F. Hamerski, M. A. Prado, V. R. Da Silva, *et al*, Kinetics of layered double hydroxide catalyzed esterification of fatty acids with glycerol, *Reaction Kinetics, Mechanisms and Catalysis*, **117**, 253 (2016).
4. B. F. Fortuoso, J. H. Dos Reis, R. R. Gebert, *et al*, Glycerol monolaurate in the diet of broiler chickens replacing conventional antimicrobials: Impact on health, performance and meat quality, *Microbial Pathogenesis*, **129**, 161 (2019).
5. D. W. Yu, Q. X. Jiang, Y. S. Xu, *et al*. The shelf life extension of refrigerated grass carp (Ctenopharyngodon idellus) fillets by chitosan coating combined with glycerol monolaurate, *Int. J. Biol. Macromol*., **101**, 448 (2017).
6. H. Q. Yang, X. Li, G. Q. Lu, Effect of carnauba wax–based coating containing glycerol monolaurate on decay and quality of sweet potato roots during storage, *Journal of Food Protection*, **81**, 1643 (2018).
7. H. Y. Chen, Z. X. Sun, H. Q. Yang, Effect of carnauba wax-based coating containing glycerol monolaurate on the quality maintenance and shelf-life of Indian jujube (Zizyphus mauritiana Lamk.) fruit during storage, *Sci. Hortic*., **244**, 157 (2019).
8. P. M. Schlievert, S. H. Kilgore, K. S. Seo, *et al*, Glycerol monolaurate contributes to the antimicrobial and anti-inflammatory activity of human milk, *Scientific Reports*, **9**, 1 (2019).
9. H. X. Zheng, L. L. Deng, F. Que, *et al*, Physical characterization and antimicrobial evaluation of glycerol monolaurate organogels, *Colloids and Surfaces A: Physicochemical and Engineering Aspects***,** **502**, 19 (2016).
10. M. S. Zhang, A. Sandouk, J. C. D. Houtman, Glycerol Monolaurate (GML) inhibits human T cell signaling and function by disrupting lipid dynamics, *Scientific Reports*, **6**, 30225 (2016).
11. Q. S. Li, J. D. Estes, P. M. Schlievert, *et al*, Glycerol monolaurate prevents mucosal SIV transmission, *Nature*, 458(7241), 1034 (2009).
12. A. Z. Abdullah, Z. Gholami, M. Ayoub, *et al*, Selective monolaurin synthesis through esterification of glycerol using slfated zirconia-loaded SBA-15 catalyst, *Chem. Eng. Commun*., **203**, 496 (2016).
13. Q. Shu, B. L. Yang, H. Yuan, *et al*, Synthesis of biodiesel from soybean oil and methanol catalyzed by zeolite beta modified with La^{3+}, *Catal. Commun.*, **8**, 2159 (2007).
14. L. Hermida, A. Z. Abdullah, A. R. Mohamed, Synthesis of monoglyceride through glycerol esterification with lauric acid over propylsulfonic acid post-synthesis functionalized SBA-15 mesoporous catalys, *Chem. Eng. J*., **174**, 668 (2011).
15. S. Kale, S. B. Umbarkar, M. K. Dongare, *et al*, Selective formation of triacetin by glycerol acetylation using acidic ion-exchange resins as catalyst and toluene as an entrainer, *Appl. Catal. A*: *Gen.*, **490**, 10 (2015).
16. Z. I. Ishak, N. A. Sairi, Y. Alias, *et al*, Production of glycerol carbonate from glycerol with aid of ionic liquid as catalyst, *Chem. Eng. J*., **297**, 128 (2016).
17. Y. Pouilloux, S. Métayer, J. Barrault, Synthesis of glycerol monooctadecanoate from octadecanoic acid and glycerol. Influence of solvent on the catalytic properties of basic oxides, Comptes Rendus de l'Académie des Sciences-Series *IIC-Chemistry*, **3**, 589 (2000).
18. C. E. Gonçalves, L. O. Laier, A. L. Cardoso, *et al*, Bioadditive synthesis from $H_3PW_{12}O_{40}$-catalyzed glycerol esterification with HOAc under mild reaction conditions, *Fuel Process. Technol*., **102**, 46 (2012).
19. W. N. R. W. Isahak, M. Ismail, N. M. Nordin, *et al*, Selective synthesis of glycerol monoester with heteropoly acid as a new catalyst, Advanced Materials Research. *Trans Tech Publications Ltd*, **545**, 373 (2012).
20. Y. J. Du, J. Gao, W. X. Kong, *et al*, Enzymatic synthesis of glycerol carbonate using a lipase immobilized on magnetic organosilica nanoflowers as a catalyst, *ACS Omega*, **3**, 6642 (2018).
21. S. Bauma, E. Ritter, I. Smirnova, *et al*, The role of phase behavior in the enzyme catalyzed synthesis of glycerol monolaurate, *RSC Adv*., **6**,

32422 (2016).

22. M. Misono, T. Okuhara, T. Ichiki, *et al*, Pseudoliquid behavior of heteropoly compound catalysts. Unusual pressure dependences of the rate and selectivity for ethanol dehydration, *J. Am. Chem. Soc*., **109**, 5535 (1987).
23. X. X. Han, K. Ouyang, C. H. Xiong, *et al*, Transition-metal incorporated heteropolyacid-ionic liquid composite catalysts with tunable Brønsted/Lewis acidity for acetalization of benzaldehyde with ethylene glycol, *Appl. Catal. A: Gen*., **543**, 115 (2017).
24. M. Y. Huang, X. X. Han, C. T. Hung, *et al*, Heteropolyacid-based ionic liquids as efficient homogeneous catalysts for acetylation of glycerol, *J. Catal.*, **320**, 42 (2014).
25. Y. Leng, J. Wang, D. R. Zhu, *et al*, Heteropolyanion-based ionic liquids: Reaction-induced self-separation catalysts for esterification, *Angewandte Chemie*, **48**, 168 (2009).
26. X. X. Han, K. K. Chen, W. Yan, *et al*, Amino acid-functionalized heteropolyacids as efficient and recyclable catalysts for esterification of palmitic acid to biodiesel, *Fuel*, **165**, 115 (2016).
27. R. Tesser, M. Di Serio, M. Guida, *et al*, Kinetics of oleic acid esterification with methanol in the presence of triglycerides, *Ind. Eng. Chem. Res*., **44**, 7978 (2005).
28. M. J. Da Silva, N. A. Liberto, L. C. D. A. Leles, *et al*, $Fe_4(SiW_{12}O_{40})_3$-catalyzed glycerol acetylation: Synthesis of bioadditives by using highly active Lewis acid catalyst, *J. Mol. Catal. A: Chem.*, **422**, 69 (2016).
29. X. X. Han, X. F. Zhang, G. Q. Zhu, *et al*, Ionic liquid–silicotungstic acid composites as efficient and recyclable catalysts for the selective esterification of glycerol with lauric acid to monolaurin, *Chem. Cat. Chem.*, **9**, 2727 (2017).
30. A. M. Zheng, S. H. Li, S. B. Liu, *et al*, Acidic properties and structure-activity correlations of solid acid catalysts revealed by solid-state NMR spectroscopy, *Acc. Chem. Res*., **49**, 655 (2016).
31. A. M. Zheng, S. B. Liu, F. Deng, ^{31}P NMR chemical shifts of phosphorus probes as reliable and practical acidity scales for solid and liquid catalysts, *Chem. Rev*., **117**, 12475 (2017).
32. A. Zheng, S. J. Huang, S. B. Liu, *et al*, Acid properties of solid acid catalysts characterized by solid-state ^{31}P NMR of adsorbed phosphorous probe molecules, *Phys. Chem. Chem. Phys*., **13**, 14889 (2011).
33. F. H. Alhassan, U. Rashid, R. Yunus, *et al*, Synthesis of ferric-manganese doped tungstated zirconia nanoparticles as heterogeneous solid superacid catalyst for biodiesel production from waste cooking oil, *Int. J. Green Energy*, **12**, 987 (2015).
34. Q. Zhang, T. Yang, X. Liu, *et al*, Heteropoly acid-encapsulated metal-organic framework as a stable and highly efficient nanocatalyst for esterification reaction, *RSC Adv*., **9**, 16357 (2019).
35. A. H. M. Fauzi, N. A. S. Amin, Optimization of oleic acid esterification catalyzed by ionic liquid for green biodiesel synthesis, Energy Conversion and Management, 76, 818 (2013).